ACS APPLIED MATERIALS & INTERFACES

Research Article

www.acsami.org

Direct Deposition of Cubic Boron Nitride Films on Tungsten Carbide–Cobalt

Kungen Teii*,† and Seiichiro Matsumoto†,‡

†Department of Applied Science for Electronics and Materials, Interdisciplinary Graduate School of Engineering Sciences, Kyushu University, Kasuga, Fukuoka 816-8580, Japan

‡Exploratory Materials Research Laboratory for Energy and Environment, National Institute for Materials Science, 1-2-1 Sengen, Tsukuba, Ibaraki 305-0047, Japan

ABSTRACT: Thick cubic boron nitride (cBN) films in micrometer-scale are deposited on tungsten carbide–cobalt (WC-Co) substrates without adhesion interlayers by inductively coupled plasma-enhanced chemical vapor deposition (ICP-CVD) using the chemistry of fluorine. The residual film stress is reduced because of very low ion-impact energies (a few eV to ~25 eV) controlled by the plasma sheath potential. Two types of substrate pretreatment are used successively; the removal of surface Co binder using an acid solution suppresses the catalytic effect of Co and triggers cBN formation, and the surface roughening using mechanical scratching and hydrogen plasma etching increases both the in-depth cBN fraction and deposition rate. The substrate surface condition is evaluated by the wettability of the probe liquids with different polarities and quantified by the apparent surface free energy calculated from the contact angle. The surface roughening enhances the compatibility in energy between the cBN and substrate, which are bridged by the interfacial sp^2-bonded hexagonal BN buffer layer, and then, the cBN overlayer is nucleated and evolved easier.

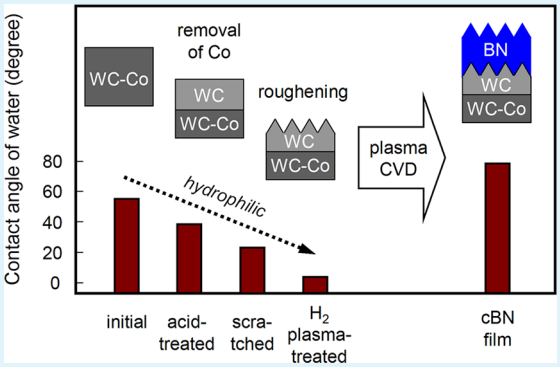

KEYWORDS: *cubic boron nitride, hexagonal boron nitride, diamond, inductively coupled plasma, plasma chemical vapor deposition, tungsten carbide, cobalt, wettability, surface free energy, roughness*

1. INTRODUCTION

Cubic boron nitride (cBN) has a number of highly attractive properties comparable to diamond such as high hardness, wide band gap, and high thermal conductivity. Among the potential advantages of cBN over diamond is that cBN is chemically inert against ferrous materials and resistant to oxidation even at high temperatures up to ~1000 °C and thus suitable for cutting iron-containing materials like steel. cBN powders synthesized by the high-temperature and high-pressure methods are used to produce various tools, by either cementing the powders with metal binders into the form of tools or brazing the powders onto cemented carbide tools. However, cBN film coatings on tool materials are still a challenge to industrial use. The limitation of the geometry and the high cost of production for cBN powder tools make it of great value to develop cBN coating tools.

It is accepted that impingement of energetic ions on the substrate surface is essential for the deposition of cBN films. The threshold ion energy is in the range of ~50 eV to a few hundreds of eV for sputtering and plasma-enhanced chemical vapor deposition (CVD) and more than a few hundreds of eV for ion beam-assisted deposition (for reviews, see refs 1 and 2). In general, the growth of a cBN layer on foreign substrates follows an initial sp^2-bonded hexagonal BN (hBN) layer typically consisting of turbostratic BN (tBN) and amorphous BN (aBN) phases. The resulting film has low crystallinity (nanometer-sized grains), high residual compressive stress (up to 20 GPa), low adhesion to the substrate, and lack of long-term stability under ambient conditions. Adherent cBN films are mostly limited within a thickness of a few hundreds of nanometers. Several groups deposited thick (over 1 μm) cBN films on Si by reducing the film stress and/or introducing adhesion interlayers.[3−7]

Deposition of thick cBN films on tool materials such as steel and cemented tungsten carbide–cobalt (WC-Co) is much more difficult. It is believed that cobalt as a binder in WC-Co has a catalytic effect, which promotes the formation of sp^2BN phase and inhibits the formation of cBN phase. Also, a relatively high solubility of boron into cobalt hinders the formation of an adherent interfacial alloy and decreases the adhesion of a film. Several groups tried to find a route to thick and adherent cBN films on WC-Co by introducing adhesion interlayers such as B-rich BN,[8] graded BCN→BN,[9] and diamond.[10] Keunecke et al. deposited 1.2 μm-thick cBN films on WC-Co cutting inserts with TiN (or TiAlN)/graded BCN→BN interlayer systems and demonstrated the high potential of cBN coatings in the turning

Received: July 1, 2012
Accepted: September 5, 2012
Published: September 5, 2012

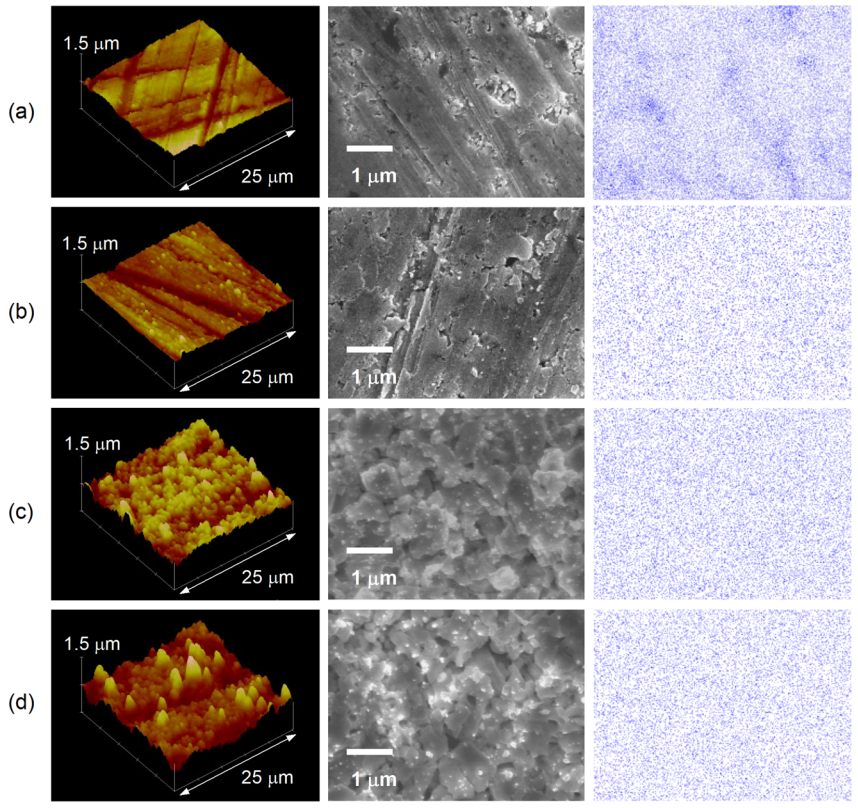

Figure 1. AFM (left column) and SEM (center column) images and the EDS mapping patterns of Co (right column) corresponding to the SEM images for the (a) initial, (b) acid-treaded, (c) scratched, and (d) H-treated substrates.

and milling tests.[11] On the other hand, a few groups reported the deposition of cBN films on WC-Co without adhesion interlayers,[12−14] but they have not obtained thick and adherent cBN films.

The introduction of the chemistry of fluorine into the CVD process in a plasma jet by the work of Matsumoto and Zhang enabled one to produce very thick (over 20 μm) and adherent cBN films on Si,[15,16] but the high-pressure (6.7 kPa) and high-temperature (~1000 °C) conditions may provide low controllability and limited applicability. In the previous work, we demonstrated a way to deposit cBN films on Si under very low-energy ion bombardment by CVD in a low-pressure inductively coupled plasma (ICP) with the chemistry of fluorine.[17] The threshold ion energy and deposition temperature were reduced to a few eV and 730 °C, respectively. The resulting film consisted of micrometer-sized grains with crystallographic morphology with the in-depth cBN fraction up to 70 vol %.[18−20] For Si substrates, the cBN fraction increased with increasing initial surface roughness of the substrate,[21] wholly opposed to the result for ion-beam deposition with 150 eV ions.[22] This suggests that the nucleation energetics under such soft ion impact depends strongly on the *apparent* surface free energy of the substrate, i.e., the surface free energy per unit area multiplied by the actual surface area.

In the present work, an attempt is made to deposit cBN films directly on WC-Co under very low-energy ion bombardment by ICP-CVD with the chemistry of fluorine. The surface condition of WC-Co generally depends upon many factors such as sintering and polishing procedures. Here, the WC-Co surface is modified with chemical and mechanical treatments and evaluated by wetting behavior of the probe liquids with difference polarities. We try to explain the mechanism for direct deposition of thick films in terms of free energies of the film, substrate, and interface.

2. EXPERIMENTAL SECTION

2.1. Deposition. BN Films were deposited in the high-density source region of an ICP with a three-turn helical copper antenna wound around a silica glass tube of 50 mm in inside diameter and 350 mm in length.[17] A sintered BN tube 45 mm in inside diameter was suspended to suppress both impurities from the silica tube and capacitive coupling between the coil and plasma. A mixture of He, N_2, H_2, and 10 vol % BF_3 diluted in He at flow rates of 80, 10, 10, and 18 sccm (i.e., 1.8 sccm of BF_3 and 16.2 sccm of He in total 18 sccm), respectively, was used. The radio frequency plasma power at 13.56 MHz and total pressure were kept at 1 kW and 40 Pa. The substrate was heated by plasma without a heater, and its temperature was measured to be 730 ± 20 °C with an infrared pyrometer. The electron density near the substrate measured with a Langmuir probe was around 3×10^{11} cm^{-3}. A positive direct-current bias (V_s) was applied to the substrate in reference to the grounded stainless steel reactor. The mean ion-impact energy was controlled by the sheath potential, which is defined by a difference between the plasma potential and the substrate bias V_s. The sheath potential decreased from 45 V to a few V or less with increasing V_s due to a shift up of the plasma potential.[17,23] The sheath potentials were 25, 10, and below 3 V at V_s = +30, 50, and +70 V, respectively.[17] WC-6 wt % Co substrates ($11.5 \times 11.5 \times 1.0$ mm^3) were produced by sintering, polished by grinding, and cleaned with acetone and ethanol in an ultrasonic bath (hereafter, called "initial"). The actual coating area was limited to about 1 cm in diameter by the sintered BN frame cover of the substrate holder. Prior to deposition, the following three types of pretreatment were made on the substrates: (1) dipping in a 10% HNO_3 solution to remove the Co binder near the surface, followed by an ultrasonic cleaning with ethanol ("acid-treated"), (2) dipping in a 10% HNO_3 solution and random scratching with emery paper to roughen the surface, followed

dx.doi.org/10.1021/am301133d | ACS Appl. Mater. Interfaces 2012, 4, 5249−5255

by an ultrasonic cleaning with ethanol ("scratched"), and (3) dipping in a 10% HNO_3 solution, random scratching with emery paper, and exposure to a pure H_2 ICP with V_s = +40 V at ~700 °C for 30 min to further roughen the surface in microscopic-scale ("H-treated").

2.2. Characterization. For structural characterization of the substrates and films, atomic force microscopy (AFM), scanning electron microscopy (SEM) equipped with energy-dispersive X-ray spectroscopy (EDS), Fourier transform infrared spectroscopy (FTIR), and glancing-angle X-ray diffraction (GXRD) were used. AFM images were captured in tapping mode at room temperature in atmosphere using Si tip probes with the radius of curvature of 10 nm. FTIR was performed in a reflection mode using s-polarized light with an incident angle of 75°. The film thickness was measured from a step height with a stylus profilometer. For thick films (>~1 μm), it was calculated from interference fringes in FTIR spectra with the refractive index of 2.1 for cBN[1] to avoid the effect of substrate deformation. The wetting property of the substrates and films was characterized by contact angle measurement of the probe liquids via sessile-drop technique. A droplet of deionized water, ethylene glycol, or 1-bromonaphthalene with a volume of 3 μL was placed onto the surface from a syringe needle, and then, the morphology of the drop was observed with a charge-coupled-device camera. The lower measurable limit of contact angle was between 1.5° and 2.0°.

3. RESULTS

3.1. Characterization of the WC-Co Substrates. AFM and SEM images and the EDS mapping patterns of Co corresponding to the SEM images for the initial, acid-treaded, scratched, and H-treated substrates are shown in Figure 1a–d. The initial surface consists of a large number of linear trenches, of which width and depth are smaller than the order of subμm and μm, respectively. The trenches are introduced randomly by grinding and mostly pointed to one to a few directions within the observed images. The Co binder exists nonuniformly over the surface such that it is occasionally aggregated to form μm-sized mottled patterns in the EDS pattern. The acid-treated surface shows a similar morphology to the initial one except the appearance of a lot of subμm-sized particles assigned to WC because of removal of surface Co binder as shown in the EDS pattern. The root-mean-square (rms) roughness measured at a few locations on the surface remains almost constant at 89 ± 7 and 90 ± 5 nm for the initial and acid-treated surfaces, respectively. The scratched surface shows a quite different morphology such that the trenches are obscured and the subμm- to μm-sized granular structures dominate the surface, accompanied by a large increase in rms roughness to around 160 nm. The H-treated surface is dominated by subμm- to μm-sized granular structures similar to the scratched one, with a further increase in rms roughness to around 240 nm. In general, the roughness after plasma etching depends upon the ratio of anisotropic to isotropic etching rate.[21,24] Hydrogen ions collide with a surface vertically with the kinetic energy much higher than the thermal energy and etch it along their incidence, leading to anisotropic etching. The positive biasing minimizes ion-induced damage. Hydrogen atoms migrate on a surface laterally and etch it along their migration path, leading to isotropic etching. The roughness was found to be increased the most with V_s = +40 V for WC-Co in our study.

EDS spectra for the initial, acid-treaded, scratched, and H-treated substrates are shown in Figure 2. The Co concentration near the surface of the initial substrate is about 4 wt %. Microscopically, the in-plane distribution of Co is nonuniform as shown in Figure 1a. The signal intensity of Co is reduced to as low as the noise level (below 0.2 wt %Co) after dipping in the acid solution with disappearance of the mottled patterns as shown in Figure 1b. The Co concentration remains negligibly low even after the scratching and H_2 plasma treatments as shown in Figure 1c,d. The detection depth of EDS is referred to the projected range of electrons (Z_m) given by the Castaing's equation:[25]

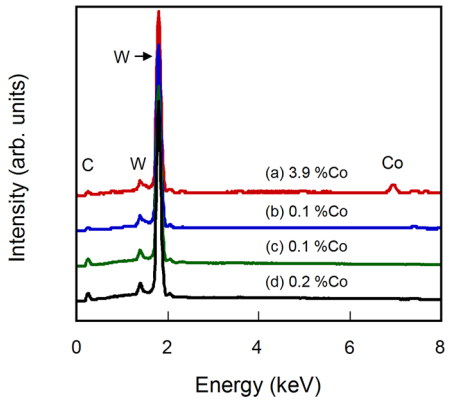

Figure 2. EDS spectra corresponding to the SEM images in Figure 1 for the (a) initial, (b) acid-treaded, (c) scratched, and (d) H-treated substrates.

$$Z_m = 0.033(V_0^{1.7} - V_c^{1.7})A/\rho Z \quad (1)$$

where V_0 is the acceleration voltage of electrons in keV, V_c is the critical voltage for emitting characteristic X-ray of each element in keV, A is the atomic mass of matrix, ρ is the mass density of matrix, and Z is the atomic number of matrix. Using eq 1, the Z_m value is estimated to be 1.1 μm for Co Kα (6.924 keV) in a W matrix at V_0 = 20 keV. The great reduction of Co in the results of EDS is reasonable since the maximum etching depth after dipping in the acid solution estimated by SEM is more than 2 μm.

3.2. Characterization of the BN Films. FTIR reflection spectra of the films deposited on the initial, acid-treaded, scratched, and H-treated substrates with V_s = +30, +50, and +70 V are shown in Figures 3a–d. The deposition time is 45 min for V_s = +30, +50, and +70 V and exceptionally 30 min for V_s = +30 V in Figure 3d. The absorption peaks at around 780, 1370, and 1600 cm^{-1} are attributed to sp^2-bonded hBN, while the absorption peak at 1050–1090 cm^{-1} is the transverse optical mode of sp^3-bonded cBN. The sp^2BN peak at around 1370 cm^{-1} is overlapped with the longitudinal optical mode of cBN at 1310–1340 cm^{-1}. For the initial surface (Figure 3a), the films with V_s = +30 and +70 V consist only of sp^2BN, while that with V_s = +50 V contains a small amount of cBN. The deposition rate is low at ~7 nm/min, and the resulting film thickness is 0.3 μm for V_s = +50 V. For the acid-treaded surface (Figure 3b), the films consist of sp^2BN and cBN. The in-depth fraction of cBN is lower than that of sp^2BN because the intensity of the cBN peak at 1050–1090 cm^{-1} is much weaker than that of the sp^2BN peak at ~1600 cm^{-1}. The deposition rate is still low at ~11 nm/min, and the resulting film thickness is 0.5 μm for V_s = +50 V. For the scratched surface (Figure 3c), the intensity of the cBN peak at 1050–1090 cm^{-1} approaches or exceeds that of the sp^2BN peak at ~1600 cm^{-1}. The deposition rate and resulting film thickness are increased to ~27 nm/min and 1.2 μm for V_s = +50 V. For the H-treated surface (Figure 3d), the cBN fraction is apparently higher than that for the scratched surface because the intensity of the cBN peak at 1050–1090 cm^{-1} is stronger than that of the sp^2BN peak at ~1600 cm^{-1}, similar to the result for roughened Si

dx.doi.org/10.1021/am301133d | ACS Appl. Mater. Interfaces 2012, 4, 5249–5255

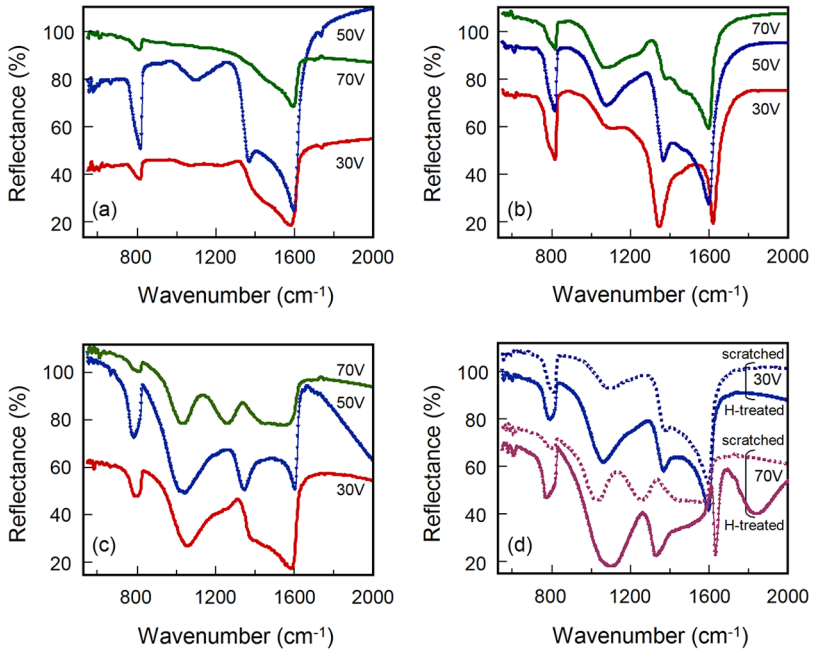

Figure 3. FTIR reflection spectra of the films deposited on the (a) initial, (b) acid-treaded, (c) scratched, and (d) H-treated substrates with V_s = +30, +50, and +70 V. For (d), the spectra of the films for the scratched substrates are given for comparison.

substrates.[21] For the H-treated surface, the deposition rate and resulting film thickness reach ~33 nm/min and 2.0 μm for V_s = +70 V, which are more than 4 times larger than ~7.5 nm/min and 0.45 μm for the scratched surface. The in-depth cBN fraction is estimated to be ~65 vol % for V_s = +70 V with the IR absorption coefficients of cBN and sp^{2}BN[21] if the method of calculation in transmittance mode is applicable. Thus, the removal of Co using an acid solution triggers cBN formation. The roughening using the scratching and H_2 plasma treatments increases both the cBN fraction and the deposition rate, wholly opposed to the result for ion-beam deposition with 150 eV ions.[22]

The substrate bias current onto the scratched substrate measured in a pure He ICP as a function of V_s is shown in Figure 4a. Pure He was used to avoid the effect of deposits, but the result well represents that for the He−N_2−H_2−BF_3 mixture. The majority of bias current during deposition is electron current because electron current increases exponentially and ion current decreases gently when V_s is increased above the floating potential at net zero current, similar to a Langmuir probe characteristic. In Figure 4a, the electron current is estimated by subtracting the ion current, which is the linear extrapolation of the ion saturation current to the positive bias voltage region. The substrate bias current onto the scratched substrate measured in the He−N_2−H_2−BF_3 ICP as functions of deposition time and V_s (+30, +50, and +70 V) is shown in Figure 4b. The film thickness values measured at five conditions are given together. At the start of deposition, the ion current density onto the coating area of about 1 cm in diameter remains at ~24 mA/cm^2, while the electron current density increases from ~90 to 320 mA/cm^2 with increasing V_s. During deposition, the initial small rise in bias current can be attributed to removal of residual impurities or adsorbates on the substrate. The bias current decreases gradually with deposition time and then is saturated when the film thickness becomes micrometer-scale due to higher electrical resistance of the films. The ion flux onto the growing thick (≥~1 μm) film is only below some 10%

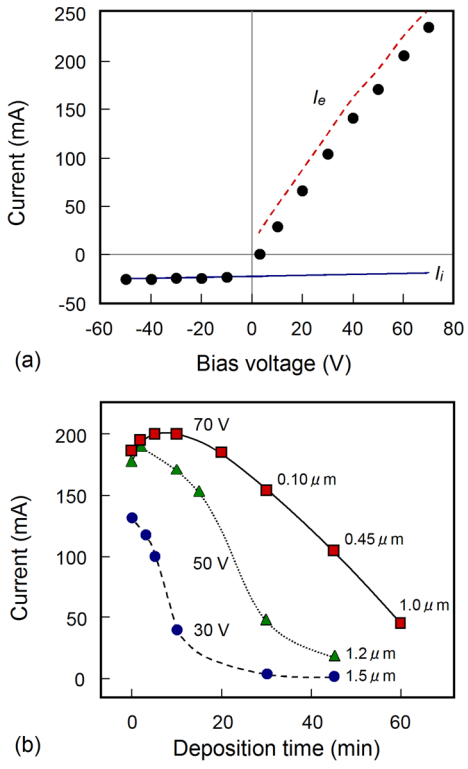

Figure 4. (a) Substrate bias current onto the scratched substrate in a pure He ICP as a function of V_s. (b) Substrate bias current onto the scratched substrate in the He−N_2−H_2−BF_3 ICP as functions of deposition time and V_s. The film thickness values at five conditions are given together. I_e and I_i are the electron and ion currents, respectively.

of that onto the pristine substrate. This is not problematic for Si substrates since the film thickness without delamination is limited within ~1 μm. The decreasing ion flux decreases the deposition rate and the fraction and crystallinity of cBN toward the growth direction. In fact, FTIR revealed that the amount of

sp^2BN tends to increase for the film thickness above ~1 μm, dissimilar to sp^2BN/cBN layered structures typical for cBN films.

GXRD patterns of the films deposited with V_s = +30, +50, and +70 V on the scratched substrate are shown in Figure 5.

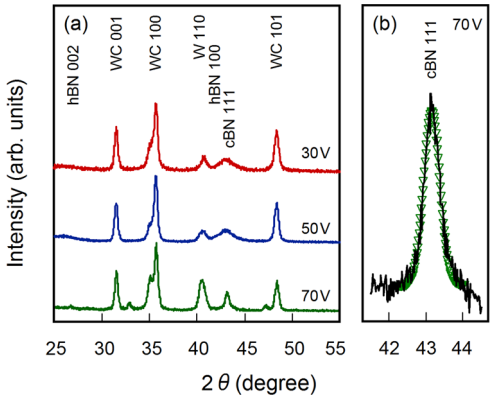

Figure 5. (a) GXRD patterns of the films deposited with V_s = +30, +50, and +70 V on the scratched substrate. (b) Typical Lorentzian fit of the peak near 2θ = 43° for the film with V_s = +70 V in (a).

The film thickness is about 1.2, 1.5, and 0.45 μm for V_s = +30, +50, and +70 V, respectively. The X-ray incidence is set below 0.5°, so the measurement gives information on the surface to bulk. All patterns exhibit distinct diffractions from WC, W, and cBN, while no diffractions from borides and nitrides are observed. Diffractions of sp^2BN (hBN) are very weak as the sp^2BN phase is highly disordered or amorphous and, hence, the primary hBN{002} peak normally at 26.79° is almost absent. The cBN{111} peak at around 43° is broadened for V_s = +30 and +50 V, while it is well distinguished for V_s = +70 V. The broadening of the cBN peak can be attributed to deterioration of the crystallinity by the decreasing ion flux onto thicker films, not to overlap of the hBN{100} and {101} peaks normally at 41.63° and 43.91°. For V_s = +70 V, the apparent crystal size is calculated to be 22 nm from the fwhm (0.55°) of the cBN{111} peak using the Scherrer's equation. The calculated size is as large as that for a high-quality cBN film deposited on Si in a plasma jet[15,20] and should be underestimated due to a number of structural defects such as stacking faults and twins.[26] Assuming a biaxial stress and neglecting shear components in the film, the residual stress is roughly estimated from the cBN{111} peak position using the Young's modulus and the Poisson's ratio.[26,27] For V_s = +70 V, it is compressive and calculated to be 4.0 GPa.

Top-view low and high magnification SEM images of the film about 0.45 μm thick, deposited with V_s = +70 V on the scratched substrate, are shown in Figure 6a,b. The corresponding 10 × 10 μm^2 AFM image is shown in Figure 6c. The film surface consists of submicrometer- to micrometer-sized grains and occasionally shows small pits with sizes below some tens of nanometers. No apparent delamination of the film is observed over the whole surface. The rms roughness of the film calculated from a 25 × 25 μm^2 AFM image (not shown) is around 250 nm, which is much larger than around 160 nm for the scratched substrate. This is due to the three-dimensional island growth, referred to as Volmer–Weber mode, under very low-energy ion bombardment. The high magnification SEM image clearly shows that a number of small subgrains with sizes

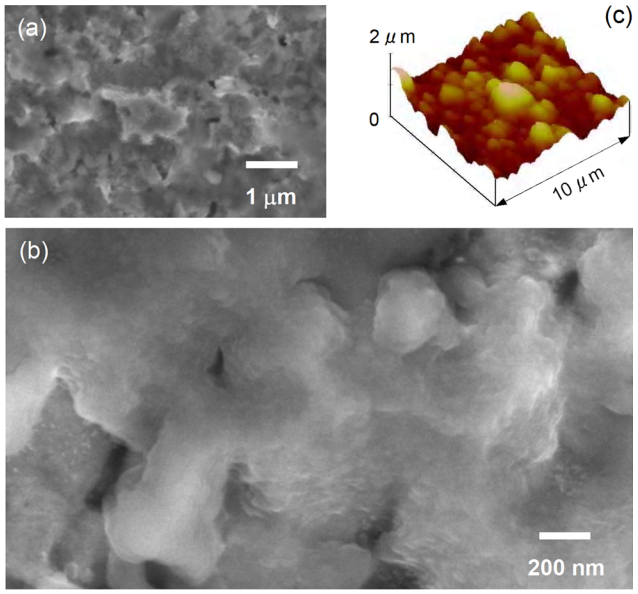

Figure 6. (a) Low and (b) high magnification SEM images of the film deposited with V_s = +70 V on the scratched substrate. (c) 10 × 10 μm^2 AFM image corresponding to the SEM images.

of several tens of nanometers are aggregated densely to form a continuous granular film.

3.3. Wettability and Surface Free Energies of the WC-Co Substrates and BN Films. The contact angle of water, ethylene glycol, and 1-bromonaphthalene for the initial, acid-treaded, scratched, H-treated substrates, and the film deposited with V_s = +70 V on the scratched substrate is shown in Figure 7. The rms roughness values calculated from 25 × 25 μm^2 AFM

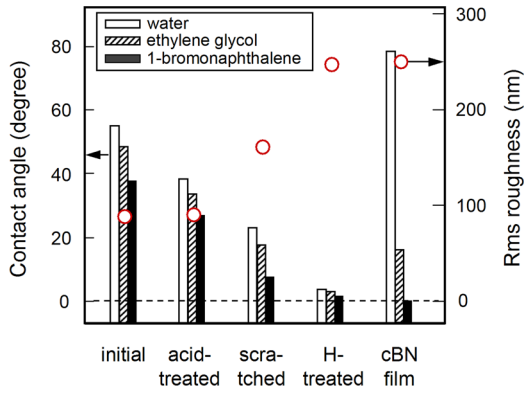

Figure 7. Contact angles of water, ethylene glycol, and 1-bromonaphthalene (open, shaded, and filled bars) for the initial, acid-treaded, scratched, H-treated substrates, and the film deposited with V_s = +70 V on the scratched substrate. The rms roughness values are given together (open circles).

images are given together. The contact angle was measured a few times at different locations to obtain an average value, and the spread of the value arising from the in-plane nonuniformity was within ±2°. Both surface free energy and polarity are larger in the order of water, ethylene glycol, and 1-bromonaphthalene. In Figure 7, the contact angle of water is the largest among the three liquids for a given surface because of the highest surface free energy. The wetting behavior of the three liquids shows the same tendency; that is, the contact angle of each liquid decreases with increasing duration of the substrate pretreat-

dx.doi.org/10.1021/am301133d | ACS Appl. Mater. Interfaces 2012, 4, 5249–5255

ment. The initial substrate has a contact angle of water of ~55°, so the surface is not hydrophilic. The acid-treated substrate shows a decrease in contact angle although the surface rms roughness remains almost constant. The contact angle of water for the H-treated substrate decreases down to 3.8°, so the surface becomes hydrophilic. On the other hand, the cBN films have high contact angles of water, typically in the range of 60° to 85° depending upon the substrate treatment and bias, so the surface is rather hydrophobic. The contact angle for the sp^2BN films was similar to that for the cBN films.

A contact angle can be used as a measure of an *apparent* surface free energy; the lower the contact angle becomes, the higher the apparent surface free energy is. An apparent surface free energy for a given area generally increases with surface roughness since the effective microscopic surface area in contact with a droplet would increase. Table 1 shows the dispersion (γ^d) and polar (γ^p) components of the apparent surface free energy ($\gamma^* = \gamma^d + \gamma^p$) of the initial, acid-treaded, scratched, and H-treated substrates and the film deposited with V_s = +70 V on the scratched substrate, calculated from the contact angle of water and 1-bromonaphthalene using the Owen and Wendt method.[28] For calculation, 1-bromonaphthalene was used as an apolar liquid to determine the value of γ^d on a given surface, and water was used as a polar liquid to determine the value of γ^p with the already calculated value of γ^d. The values of γ^d and γ^p of water and 1-bromonaphthalene were cited from the literature.[28,29] In Table 1, both the values of γ^d and γ^p on the substrate increase with increasing duration of the substrate pretreatment. The value of γ^d ranges from 35 mJ/m^2 for the initial substrate to 44 mJ/m^2 for the H-treated substrate, while that of γ^p is in a wider range of 17 to 34 mJ/m^2. The calculation using the contact angle of water and ethylene glycol resulted in the same trend. The increase in both γ^d and γ^p is attributed to increasing surface roughness. Some portion of the increase in γ^p could be due to formation of more polar bonds and/or removal of contaminants and oxides from the surface. On the other hand, the value of γ^d on the cBN film is large, due to the high mass density of cBN, and presumably larger than that calculated here as the contact angle of 1-bromonaphthalene is below the measurable limit (<~2°). The very small value of γ^p is the major origin of hydrophobicity. This is reasonable because a large portion of the as-deposited film surface would be stabilized with strong B−F bonds.[16,17]

Table 1. Apparent Surface Free Energy (γ^*), Dispersion (γ^d), and Polar (γ^p) Components of the Initial, Acid-Treated, Scratched, and H-Treated Substrates and the cBN Film Deposited with V_s = +70 V on the Scratched Substrate

	initial	acid-treated	scratched	H-treated	cBN film
γ^* (mJ/m^2)	52.4	64.4	73.5	78.2	47.3
γ^d (mJ/m^2)	35.2	39.3	43.5	44.0	44.0[a]
γ^p (mJ/m^2)	17.2	25.1	30.0	34.2	3.3

[a]The value of γ^d for the cBN film would actually be larger, as the contact angle of 1-bromonaphthalene is below the measurable limit (<~2°).

4. DISCUSSION

The results demonstrate that cBN films up to 2.0 μm thick were deposited directly on WC-Co under very low-energy ion bombardment by applying two types of substrate pretreatment. As the catalytic effect is suppressed by removal of surface Co, cBN starts to be formed, but the amount of cBN is still smaller than that of sp^2BN. As the surface roughness is increased, cBN becomes dominant over sp^2BN accompanied by an increase in the deposition rate. For low ion energies (below ~25 eV), the surface roughening gives profound effects because the deposition is governed by surface processes of radicals assisted by soft ion impact,[17] which is largely different from subsurface processes of energetic ions typical for high ion energies (above ~50 eV).

Formation of the initial sp^2BN layer typically up to several tens of nanometers thick is the fundamental characteristic of cBN film deposition, regardless of the deposition technique and ion energy range. A number of relevant studies have tried to elucidate the origin of the sp^2BN layer. Common to these studies is that cBN nucleation occurs on aBN/tBN interfacial layers (i.e., substrate/aBN/tBN/cBN), where some portion of the basal planes of tBN are oriented nearly perpendicular to the substrate surface.[30−32] Yang et al. showed that the aBN layer containing 10−20 at % oxygen is formed on a native Si oxide layer on a Si substrate and eliminated by removal of the Si oxide layer.[33] They also observed a contraction of the interplanar spacing of the tBN basal planes between the cBN and Si substrate due to the compression of tBN.[34] The nucleation sites of cBN on the top of the preferentially oriented tBN are still open to debate, although an interplanar alignment of $(111)_{cBN}//(0002)_{tBN}$ has been suggested with approximately 3:2 lattice registry. On the basis of the above studies, the sp^2BN layer serves as the buffer medium to accommodate the different properties of the cBN and substrate; that is, lattice constant in one aspect and surface free energy in the other aspect. For polycrystalline films, we should take notice of the latter.

Nucleation of an overlayer on a surface occurs with no potential barriers when the wetting condition is satisfied[35]

$$\gamma_s > \gamma_i + \gamma_o \quad (2)$$

where γ_s and γ_o are the surface free energy of the substrate and overlayer, respectively, and γ_i is the free energy of the interface. For diamond nucleation on Si with a SiC interface, eq 2 can be satisfied by saturation of the surface dangling bonds of diamond with hydrogen, resulting in an effective slight negative surface energy.[36] The value of γ_o for the cBN overlayer (or nuclei) would be much closer to >47 mJ/m^2 measured for the cBN films than ~4.8 J/m^2 calculated for a bare cBN{111} surface.[37] The interfacial sp^2BN layer is formed with structural inhomogeneity and orientation toward the growth direction to be compatible with both the cBN and substrate and reduce the total interfacial energy given by the sum of the free energy and the bond energies of the cBN/sp^2BN and sp^2BN/substrate interfaces. The value of γ_i for the sp^2BN layer would be much smaller than its surface free energy of ~50 mJ/m^2 measured for the sp^2BN films due to bonding with the cBN and substrate. As the value of γ_s for the WC-Co substrate is increased by the roughening, from ~52 mJ/m^2 for the initial substrate up to ~78 mJ/m^2 for the H-treated substrate, the system approaches the wetting condition. Then, the cBN nuclei can be formed and evolved easier due to the lower potential barrier. The sp^2BN layer thickness becomes smaller because the energy compatibility between the cBN and substrate is more achieved, as reported for diamond[38] and roughened Si substrates.[21] The mechanism of increasing deposition rate in the subsequent stage is unclear yet. We speculate that the larger roughness increases the local electric field and attracts the more ion flux

even for thick films, enabling the higher deposition rate and larger film thickness.

The decrease in residual film stress with very low-energy ions is mainly responsible for the thick films without delamination in the air over two years even after drips of water. The substrate surface roughening is expected to increase the adhesion of the films by the anchor effect. Currently, the scratch test using a 50 μm-radius diamond tip reveals the critical load of at most a few N, which is lower than $\geq\sim$15 N typical for tool applications. The adhesion would be improved by controlling the transition from the substrate to the film. Future work should focus on engineering the structure and composition of the transition layer for strengthening the adhesion.

5. CONCLUSIONS

The ICP-CVD technique with very low ion-impact energies enabled one to deposit thick cBN films on WC-Co substrates without adhesion interlayers by applying two types of substrate pretreatment. The removal of surface Co binder suppressed the catalytic effect of Co and triggered cBN formation, and the subsequent surface roughening increased both the in-depth cBN fraction and deposition rate. For thicker films ($>\sim$1 μm), the cBN fraction and deposition rate had a tendency to decrease due to the decrease in incident ion flux onto the more resistive films. The apparent surface free energy of the substrate calculated from the contact angle of the probe liquids increased with increasing the surface roughness. The roughening increased the compatibility in energy between the cBN and substrate through the sp^2BN buffer layer and allowed the system to approach the wetting condition with the lower potential barrier to nucleation.

AUTHOR INFORMATION

Corresponding Author

*E-mail: teii@asem.kyushu-u.ac.jp.

Notes

The authors declare no competing financial interest.

ACKNOWLEDGMENTS

This work was supported in part by Industrial Technology Research Grant Program in 2008 from New Energy and Industrial Technology Development Organization (NEDO) of Japan and Funding Program for Next Generation World-Leading Researchers (NEXT Program) from Cabinet Office, Government of Japan. The authors would like to thank T. Hori for cooperation in the experiments.

REFERENCES

(1) Mirkarimi, P. B.; McCarty, K. F.; Medlin, D. L. *Mater. Sci. Eng., R: Rep.* **1997**, *21*, 47−100.
(2) Kulisch, W.; Ulrich, S. *Thin Solid Films* **2003**, *423*, 183−195.
(3) Barth, K.-L.; Lunk, A.; Ulmer, J. *Surf. Coat. Technol.* **1997**, *92*, 96−103.
(4) Litvinov, D.; Clarke, R. *Appl. Phys. Lett.* **1999**, *74*, 955−957.
(5) Boyen, H.-G.; Widmayer, P.; Schwertberger, D.; Deyneka, N.; Ziemann, P. *Appl. Phys. Lett.* **2000**, *76*, 709−711.
(6) Yamamoto, K.; Keunecke, M.; Bewilogua, K. *Thin Solid Films* **2000**, *377−378*, 331−339.
(7) Ulrich, S.; Nold, E.; Sell, K.; Stüber, M.; Ye, J.; Ziebert, C. *Surf. Coat. Technol.* **2006**, *200*, 6465−6468.
(8) Setsuhara, Y.; Kumagai, M.; Suzuki, M.; Miyake, S. *Surf. Coat. Technol.* **1999**, *116−119*, 100−107.
(9) Keunecke, M.; Yamamoto, K.; Bewilogua, K. *Thin Solid Films* **2001**, *398−399*, 142−149.
(10) Chong, Y. M.; Zhang, W. J.; Yang, Y.; Ye, Q.; Bello, I.; Lee, S. T. *Diamond Relat. Mater.* **2009**, *18*, 1387−1392.
(11) Keunecke, M.; Wiemann, E.; Weigel, K.; Park, S. T.; Bewilogua, K. *Thin Solid Films* **2006**, *515*, 967−972.
(12) Ikeda, T.; Kawate, Y.; Hirai, Y. *J. Vac. Sci. Technol., A* **1990**, *8*, 3168−3174.
(13) Weissmantel, S.; Reisse, G. *Diamond Relat. Mater.* **2001**, *10*, 1973−1982.
(14) Yu, J.; Matsumoto, S. *J. Mater. Res.* **2004**, *19*, 1408−1412.
(15) Matsumoto, S.; Zhang, W. J. *Jpn. J. Appl. Phys. Part 2* **2000**, *39*, L442−L444.
(16) Zhang, W. J.; Jiang, X.; Matsumoto, S. *Appl. Phys. Lett.* **2001**, *79*, 4530−4532.
(17) Teii, K.; Yamao, R.; Yamamura, T.; Matsumoto, S. *J. Appl. Phys.* **2007**, *101*, 033301.
(18) Teii, K.; Matsumoto, S.; Robertson, J. *Appl. Phys. Lett.* **2008**, *92*, 013115.
(19) Teii, K.; Yamao, R.; Matsumoto, S. *J. Appl. Phys.* **2009**, *106*, 113706.
(20) Teii, K.; Matsumoto, S. *J. Appl. Phys.* **2012**, *111*, 093728.
(21) Teii, K.; Hori, T.; Matsumoto, S. *Thin Solid Films* **2011**, *519*, 1817−1820.
(22) Zhou, X. T.; Sham, T. K.; Chan, C. Y.; Zhang, W. J.; Bello, I.; Lee, S. T.; Hofsäss, H. *J. Appl. Phys.* **2006**, *100*, 014909.
(23) Teii, K.; Hori, M.; Goto, T. *J. Appl. Phys.* **2001**, *89*, 4714−4718.
(24) Teii, K.; Matsumoto, S. *J. Appl. Phys.* **2007**, *101*, 013302.
(25) Castaing, R. *Adv. Electron. Electron Phys.* **1960**, *13*, 317−386.
(26) Zhang, W. J.; Matsumoto, S. *Phys. Rev. B* **2001**, *63*, 073201.
(27) Cardinale, F.; Howitt, D. G.; McCarty, K. F.; Medlin, D. L.; Mirkarimi, P. B.; Moody, N. R. *Diamond Relat. Mater.* **1996**, *5*, 1295−1302.
(28) Owens, D. K.; Wendt, R. C. *J. Appl. Polym. Sci.* **1969**, *13*, 1741−1747.
(29) Busscher, H. J.; Van Pelt, A. W. J.; De Boer, P.; De Jong, H. P.; Arends, J. *Colloids Surf.* **1984**, *9*, 319−331.
(30) Medlin, D. L.; Friedmann, T. A.; Mirkarimi, P. B.; Rez, P.; MaCarty, K. F.; Mills, M. J. *J. Appl. Phys.* **1994**, *76*, 295−303.
(31) Watanabe, S.; Miyake, S.; Zhou, W.; Ikuhara, Y.; Suzuki, T.; Murakawa, M. *Appl. Phys. Lett.* **1995**, *66*, 1478−1480.
(32) Zhang, W. J.; Matsumoto, S.; Kurashima, K.; Bando, Y. *Diamond Relat. Mater.* **2001**, *10*, 1881−1885.
(33) Yang, H. S.; Iwamoto, C.; Yoshida, T. *J. Appl. Phys.* **2003**, *94*, 1248−1251.
(34) Yang, H. S.; Iwamoto, C.; Yoshida, T. *J. Appl. Phys.* **2002**, *91*, 6695−6699.
(35) Reichelt, K. *Vacuum* **1988**, *38*, 1083−1099.
(36) Robertson, J. *Diamond Relat. Mater.* **1995**, *4*, 549−552.
(37) DeVries, R. C. *Cubic Boron Nitride: Handbook of Properties*; in Rep. 72 CRD 178; General Electric Co.: Schenectady, NY, 1972.
(38) Zhang, X. W.; Boyen, H.-G.; Deyneka, N.; Ziemann, P.; Banhart, F.; Schreck, M. *Nat. Mater.* **2003**, *2*, 312−315.